Monthly Notices
of the
ROYAL ASTRONOMICAL SOCIETY

MNRAS **444,** 2212–2217 (2014) doi:10.1093/mnras/stu1470

An Efficient Linear-array Imager for radio astronomy

Ramesh Balasubramanyam★

Raman Research Institute, Sadashivanagar, Bangalore I-560080, India

Accepted 2014 July 22. Received 2014 July 17; in original form 2013 April 4

ABSTRACT

Large-scale surveys are essential means to leapfrog astronomical understanding. Yet, Galaxy-wide surveys at millimetre wavelengths are rare and have not benefited much from multiple receivers that provide large instantaneous field of view. If one were to have a large number of millimetre wave receivers, how best to deploy them to maximize survey speed to measure both point and smoothly distributed emission? In this paper, we present a new cross telescope configuration, Efficient Linear-array Imager, and demonstrate that it provides an interesting alternate solution. As an interferometer element, it lends itself for close packing and thereby blends short and long spacing visibilities naturally, improving imaging.

Key words: instrumentation: miscellaneous – telescopes.

1 INTRODUCTION

All-sky and wide-area surveys have been important tools in enhancing our understanding of the Universe in substantial steps. Space telescopes such as *Planck* (Planck Collaboration I 2013) and *WMAP* (Larson et al. 2011) have improved our understanding of cosmology by mapping the *cosmic microwave background radiation* (CMBR) over the entire sky as did their predecessor *COBE* (Hauser et al. 1998). Other space telescopes such as *Spitzer* (Werner et al. 2004) and *IRAS* too have engaged in wide-area surveys, contributing significantly to our understanding of the objects in the Universe. Atmospheric windows in the optical and radio bands allow ground-based astronomical observations. Optical astronomers have conducted many wide-area and galactic-plane surveys (SDSS, 2MASS) in addition to surveys of catalogue objects. At lower radio frequencies too, a large number of wide-area surveys (e.g. PMMS, Cohen et al. 2007; HIPASS, Meyer et al. 2004; NVSS, Condon et al. 1998) have been carried out.

The only existing galaxy-wide spectroscopic survey in the millimetre wave window is the ^{12}CO survey conducted by Dame, Hartmann & Thaddeus (2001) at a resolution of 7.5 arcmin. The Five College Radio Astronomy Observatory (FCRAO) CO survey of the outer Galaxy at 1 arcmin resolution with the 15 element QUARRY (Heyer et al. 1998) is the next largest wide-area survey and demonstrates how multiple receivers can boost survey speed. Many multibeam, multifeed efforts have been made towards improving the instantaneous field of view (FoV; Goldsmith 1995; Payne & Jewell 1995; Payne 2002). Other modest surveys include ^{12}CO J=2→1 Nobeyama survey and the various targeted surveys undertaken with Nagoya and other telescopes, but to a limited extent and access. Surveys with molecules other than ^{12}CO are even more limited in extent (e.g. Melnick et al. 2011; Jones et al. 2012; Hacar et al. 2013) but demonstrate their importance and usefulness.

The primary reason for the paucity of millimetre wave spectroscopic surveys is the lack of wide FoV. At low frequencies, telescopes have large primary beams and therefore can aperture-synthesize reasonably large size structures (e.g. large, nearby Galaxies in line and continuum). At millimetre waves, even modest-sized telescopes have small primary beams rendering aperture synthesis less effective to trace the widely distributed molecular medium. Techniques such as heterogeneous arrays, mosaicking and joint deconvolution schemes that seamlessly incorporate the total power data from single dishes have extended the sizes to several primary beams but pointing and tracking inaccuracies do pose problems (Ekers & Rots 1979; Cornwell 1988; Sault, Staveley-Smith & Brouw 1996). Also, no large single-dish telescope with a large focal plane array (FPA) seems to have engaged in millimetre wave spectroscopic surveys except FCRAO.

There are, however, a large number of reasonably bright spectral probes of the molecular medium that dot the long (8–50 GHz) and short (80–800 GHz) millimetre spectrum and remain to be exploited on Galaxy-wide scales for improving our understanding of the interstellar medium and the star formation process. Transitions of different molecules respond differently to changes in temperature and density. Modern wideband low noise amplifier (LNA) front-ends allow many of these lines to be measured simultaneously making their ratios more accurate leading to better modelling outcomes. Accurate density and temperature maps of the interstellar medium derived by modelling multispecies spectral images at arcminute resolution using non-local thermodynamic equilibrium radiative transfer codes will be much useful and likely to throw interesting questions about the nature and distribution of molecular matter in the Galaxy.

One way to achieve this is to map the Galaxy-wide interstellar medium down to about 40 mK levels at 1 arcmin (=5 pc at 17 kpc, the other end of the molecular Galaxy) spatial and

★E-mail: ramesh@rri.res.in

1 km s^{-1} (=0.33 MHz) velocity resolution using multiple millimetre wave spectral lines (HCO^+, HCN, $N2H^+$, SiO, CS, CCS, OCS, CH3CN, ^{13}CO, ^{12}CO). This does increase the number of back-end receivers required proportional to the spectral lines to be imaged simultaneously.

For the discussion in this paper, we consider uncooled receivers for their economy and ease of operation, though cooled receivers will certainly increase the speed. Where relevant, we will comment on this aspect along the way. Assuming a single side-band system temperature, T_{sys}, of 400 K (typical for a 80–115 GHz LNA operating at room temperature in a good site) and frequency switching method to remove baseline variations, the integration time required per beam will be ∼600 s. Even to cover 2° in galactic latitude and 360° in longitude at 1 arcmin requires 2.6 million spectra. Taking 600 s per spectrum, a single pixel image will take more than 400 000 h (18 000 d or 50 yr)! Clearly, single-pixel, single-line imaging that was carried out earlier is not viable when one needs to push down the resolution by a factor of 8 and the temperature sensitivity by a factor of 3–5 to detect lines from other species. Imaging with multiple receivers is a must. The natural question is, how best to deploy the multiple receivers for surveys?

One solution is to equip telescopes with multiple beams as is the case with large millimeter telescope or earlier with FCRAO. With a 30 pixel LNA FPA on a 10 m sized telescope, the above survey time can be brought down to about 2 yr, assuming frequency switching. This is still large but manageable; cooled receivers will reduce it further to about 0.5 yr. Fast beam switching coupled with basket-weaving techniques have made imaging faint, distributed continuum emission possible with single dishes, but this is still not perfect and at the cost of time and processing overheads besides the throw limitations.

The second option is to form a synthesis telescope with the 30 receivers fitted to small 1 m antennas, with their large primary beams, distributed over 100 m^2 area. In this case, the correlations suppress baseline variations in time and frequency and therefore support observing continuum sources but at the cost of sensitivity and the increased data handling and processing overheads.

In this paper, we provide a third alternative to this issue viz. Efficient Linear-array Imager, ELI, and demonstrate its advantages over the above two methods including in efficiency and economy, even as it uses the same number of receivers. One could use this new method to modify and upgrade existing large low-frequency telescopes to high-frequency operation at modest cost, incurring minimal structural issues to solve. Realization of the imaging instrument proposed here can potentially change the way Galaxy-wide millimetre wave surveys are carried out in future.

In Section 2, the details of ELI are presented. In Section 3, the cross-power beam of ELI is calculated. In Section 4, sensitivity and survey speed of ELI is calculated in comparison to an *equivalent* single dish. In Section 5, some potential advantages of ELI as an imaging instrument are discussed in comparison to the other two ways of using multiple receivers. We conclude the paper with a summary of the results of our investigations.

2 EFFICIENT LINEAR-ARRAY IMAGER

To arrive at the ELI configuration, let us begin with the conventional paraboloid–hyperboloid two mirror system. For a circular aperture illumination, it produces a circular pencil beam on the sky. Shaping the secondary appropriately, the illumination of the paraboloid can be squeezed to an ellipse, yielding an orthogonal elliptical beam on the sky. Increasing the illumination eccentricity further, the resultant beam becomes highly elliptical or a fan-beam, as shown in Fig. 1. Now, recognizing that only a thin strip of the paraboloid is illuminated, one can replace it with a thin, long parabolic cylinder and fit it with an appropriately shaped secondary. This makes the fan-beam telescope (FBT): a long, narrow parabolic cylindrical primary, a saddle-shaped secondary and a receiver illuminating it. Such an FBT forms part of the four mirror optics scheme proposed sometime ago (Balasubramanyam 2004) to construct large telescopes economically. We follow that work to arrive at the appropriate saddle shape for the secondary. In that system, the FBT is attached to an focal pair of mirrors that acts as a beam expander and recircularizes the beam. On the other hand, ELI proposed here is a cross telescope obtained by laying two such FBTs orthogonal to each other, as shown in Fig. 2. To avoid shadowing, the secondary is shifted away from the middle (a) in the curved direction, by making the primary a slightly off-axis parabolic cylinder; (b) in the extrusion direction, by making the incidence on the primary oblique by ∼7.°5 and tilting the parabolic cylinder also to the horizontal by the same angle (for details see Balasubramanyam 2004). Further, an M-element linear receiver array is fitted to each of these FBTs, M being the aspect ratio of the fan-beam. The beam pattern of such a cross telescope is the product of the voltage beams of the two FBTs. This is similar to the well-known Mills cross *skeleton* telescope (see Christiansen & Hoegbom 1969 for details), where the fan-beam is formed by appropriately phasing a dipole array.

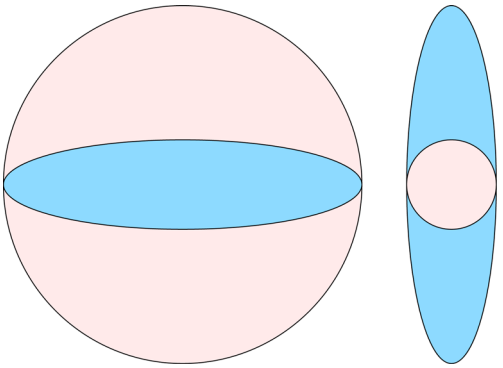

Figure 1. Left schematic shows the circular (pink) and elliptical (light blue) aperture illumination. Right schematic shows the corresponding circular and elliptical beams.

2.1 Specifications

To concretize the idea and facilitate further discussion, we present the specifications of the FBTs used in the proposed cross telescope, ELI, in Table 1. Survey being the driving force, we envisage ELI to be a transit instrument, though it can be made into a full-fledged telescope by placing the two orthogonal FBTs on a circular rail to allow azimuth tracking. Each FBT is made of a parabolic cylindrical primary and an appropriate saddle-shaped secondary that brings the radiation to a point focus. The effective focal length is enhanced which allows a large element, say 15, linear array to be used. To reduce aberrations and use the linear array efficiently, one could use hyperbolic cylindrical primary and an appropriate secondary, following Ritchey–Chretien (see Schroeder 2000) prescription.

2.2 Calculating the secondary shape

To describe the shape of the secondary surface, we need to set up a coordinate system. A convenient one is as follows: F, the final focus, is at the origin of the coordinate system; L and L', the end points

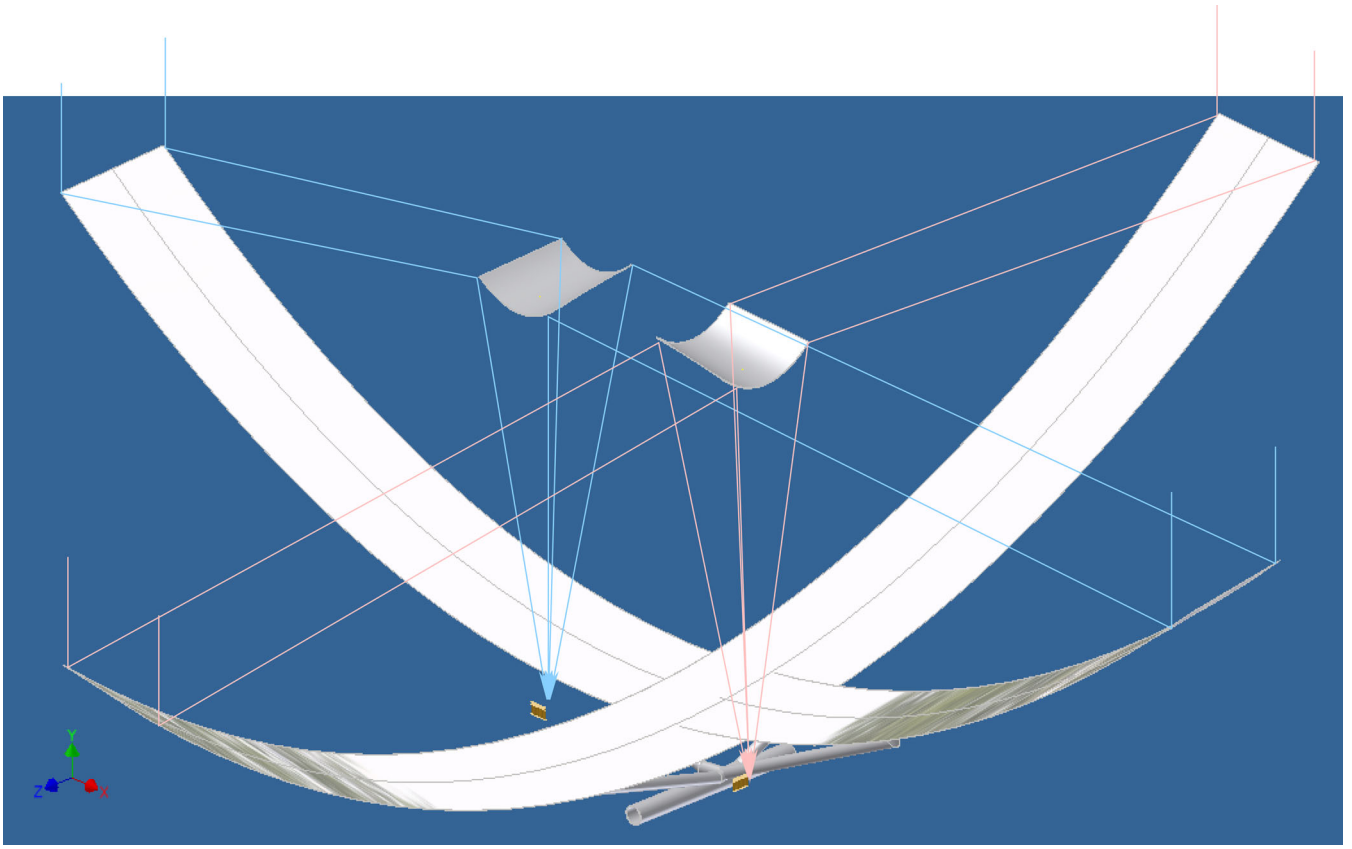

Figure 2. Schematic of the proposed cross telescope, ELI. Four corner rays incident on each arm (pink and light blue) are also shown to help visualize how the rays reach their respective foci after bouncing off their respective secondaries.

Table 1. Fan-beam telescope specifications.

Item	Specification	Comment
Primary	15 m × 1 m	Each a parabolic cylinder
f/*D*	0.3	For short secondary support
Secondary	1 m × 1 m	Saddle-shaped surface
Roughness	0.2 mm rms	Good up to 100 GHz
Linear array	15 elements	Room temperature LNAs

of the line focus formed by the primary, are given by $[-0.45, 0, f]$, $[0.55, 0, f]$, respectively; f is the focal length of the primary, given by $z = y^2/4f$, which is extruded in x between 0.05 and 1.05 m. The secondary is offset to avoid casting its own shadow on the primary. This means the rays brought to final focus are parallel rays incident on the primary at an angle $\phi = 7.^{\circ}692\,81$ away from the normal. For this configuration, the secondary surface is defined by the equation $\cos(\phi) \times (r - C) = d$, where C is a constant, ϕ is the oblique angle of incidence, r and d are shortest distances from an arbitrary point $P(x, y, z)$ on the secondary surface to the final focus $F(0,0,0)$ and to the line focus $LL^{'}$ of the primary, respectively. Constant C is adjusted to obtain a symmetrical, 1 m × 1 m secondary. Fig. 3 shows the shape of the secondary satisfying the equation for this configuration with $f = 4.5$ m and $C = 2.8$ m.

3 THE CROSS-POWER BEAM

We compute the cross-power beam by Fourier inverting the visibility function measured by the cross telescope. Imagine the aperture to be divided into many tiny square cells of side $\delta = \lambda/2$, where λ is the operating wavelength. Consider two such cells, of area $\mathrm{dA} = \delta^2$, centred at (x,y) and (x',y') in the two arms, respectively, as shown in Fig. 4. Signals from a point source reflected by these two small areas will be received by their respective receivers with the weights of $\sqrt{\frac{K}{\pi ab}}\mathrm{e}^{-((x/a)^2+(y/b)^2)K/2}$ and $\sqrt{\frac{K}{\pi ab}}\mathrm{e}^{-((x'/b)^2+(y'/a)^2)K/2}$. Here, a and b are the sides of the rectangle enclosing each reflector with an aspect ratio of $M = a/b$ and K is the grading factor used to tune the edge taper. Thus, their correlation contributes to a baseline $[u, v]$ where $u = \frac{x-x'}{\lambda}$ and $v = \frac{y-y'}{\lambda}$ with a strength equal to the product of the weights given above. By varying the centre positions

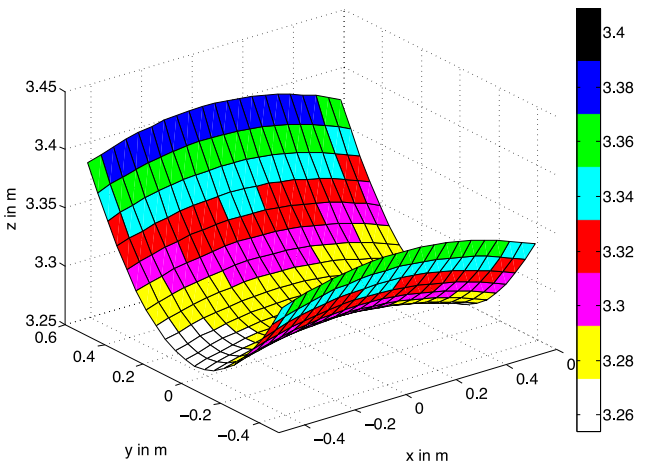

Figure 3. Shape of the secondary surface for ELI.

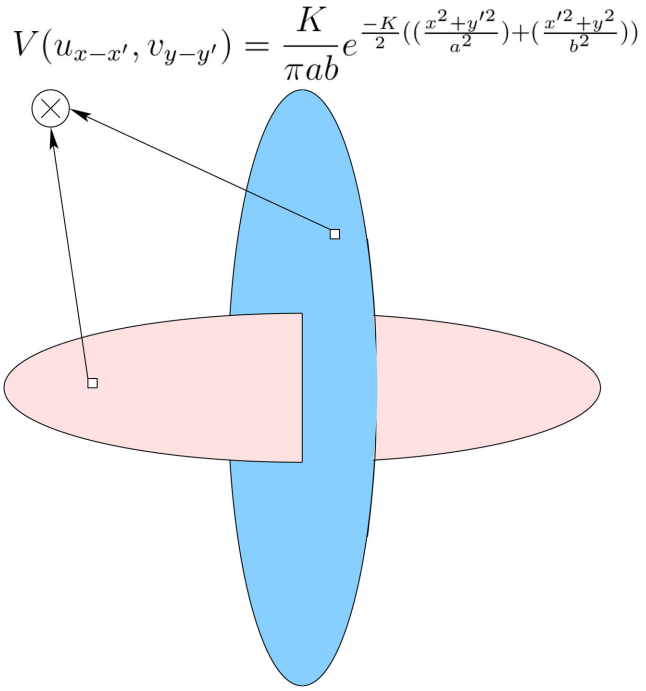

Figure 4. Schematic shows the method of finding the UV sampling of the cross telescope (pink and blue indicating the two arms) and hence obtaining the beam via Fourier inversion. Signals reflected from the two small areas contribute a visibility strength of $V(u, v) = \frac{K}{\pi ab} e^{\frac{-K}{2}((\frac{x^2+y'^2}{a^2})+(\frac{x'^2+y^2}{b^2}))}$, to the baseline $[u, v] = [\frac{x-x'}{\lambda}, \frac{y-y'}{\lambda}]$ in shaping the cross-power beam.

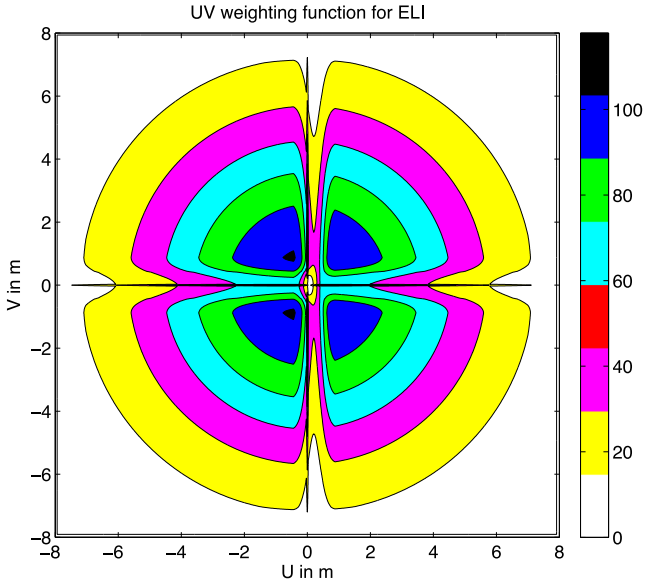

Figure 5. Visibility weighting function measured by the proposed cross telescope over the *uv* space. Here, the contour levels are relative visibility weights in arbitrary units; *u* and *v* are expressed in *m* and not in wavelength units.

of the two areas over the reflector in each arm in steps of δ and adding the correlations to the corresponding $[u, v]$ bin, one can compute the net visibility weighting function, shown in Fig. 5, that shapes each multiplicative beam. For ease of computing, we have taken $\lambda \sim 5.86$ cm, leading to 512×32 cells making up the

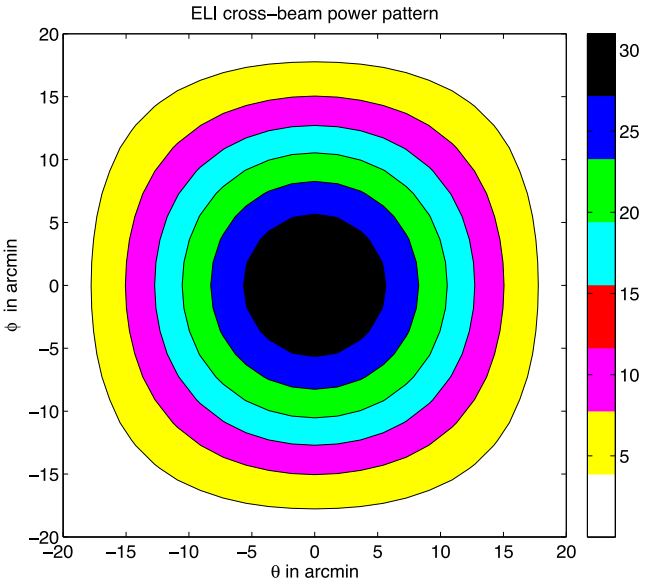

Figure 6. Beam of the proposed cross telescope. Here, the contour levels are relative beam weights in arbitrary units.

15 m × 1 m area of each FBT arm. This weighting function takes into account the small offset illumination and the central *missing area* but assumes ideal surfaces and perfect focusing. Grading factor K is taken to be 4 to yield a Gaussian illumination with a 14 dB power taper at the reflector edges. We have included contributions from *all* baselines down to $\lambda/2$ spacing. The cross-configuration ensures that short baselines too contribute to the measured cross-power spectra and therefore the telescope should respond well to large-scale distributed flux.

Fig. 6 shows the resultant cross-power beam, the Fourier transform of the above visibility weighting function. This beam applies to 5.86 cm wavelength but can be appropriately scaled to higher frequencies without loss of generality. The beam has a half-power width of 19.5 arcmin, similar to that of a 10.6 m paraboloid at 5.86 cm wavelength, though the linear dimension of ELI is 15 m on the long side. One way to see this is to look at the 15 m ELI from space as an X-form: the maximum baseline on either direction is $15/\sqrt{2} = 10.6$ m. Another way is to recognize that, for this fan-beam cross-multiplicative array, the power beam is the same size as the smaller side of the voltage fan-beam.

The proposed ELI system is more suitable at millimetre wavelengths. We recognize that making 15 beams at longer wavelengths has its share of problems: if L_λ is the secondary size in wavelength, its inverse is the angle subtended by the focal waist at the focal distance. Assuming this to be the element aperture, $15/L_\lambda$ will be the total angle subtended by all the receivers, forcing the illumination to be offset by half this angle to avoid shadowing. The distance to the final focus from the secondary can be reduced to make the waist diameter smaller but this may limit the number of beam elements (Ivashina, Bregman & van Ardenne 2002). For longer wavelengths, the eight receiver option is possibly more appropriate. Densely packed focal line array may also be considered.

4 SENSITIVITY AND SURVEY SPEED

Consider an ELI with each arm of length L and aspect ratio, M. The reflecting area, A_x, is $\pi L^2/(2M)$. Following the discussion above, the area of a single dish, A_0, with the same resolution will be,

$\pi L^2/8$. Given that antenna temperature $T_a = A_p \frac{T_B \Omega_b}{\lambda^2}$, the antenna temperature ratios between ELI and the corresponding single dish for each beam will be $\frac{T_x}{T_0} = \frac{A_x}{A_0} = \frac{4}{M}$. This means the ratio of the integration times required to achieve the same signal to noise per beam will be $16/M^2$. For $2M$ receivers, ELI makes M^2 simultaneous measurements compared to $2M$ measurements of the single dish. Therefore, the relative mapping speed ratio $\frac{A_x^2 \Omega_x}{A_0^2 \Omega_0} = \frac{8}{M}$. The left-hand side is the ratio of the common figure of merit, $(A/T_{\rm sys})^2\Omega$, for the two antennas under comparison, fitted with identical set of receivers. Following cases arise:

(A) For $M = 4$, number of receivers is eight and ELI has same reflector area as the single dish with the same angular resolution. In survey speed, ELI is twice as fast as the single dish.

(B) For $M = 8$, number of receivers is 16 and ELI has half the reflector area as the single dish with the same resolution. Then, ELI is as fast as the single dish.

(C) With $M = 16$, there are 32 receivers; ELI has $1/4$th the reflector area of the single dish with the same beam size. In this case, ELI is half as fast as the single dish.

To be precise, ELI cross-correlation output is $\sqrt{2}$ times worse in noise compared to the single dish with same area. However, in the case of a single dish one needs to employ some kind of switching to buy immunity against gain variations. Frequency switching would restore parity and above statements are valid. If one compares with position switching then the mapping speed ratio is $\frac{16}{M}$; then, case-(A) ELI will be four times faster, case-(B) ELI twice as fast and case-(C) ELI will achieve parity in imaging speed in relation to a single dish of same resolution. The notable aspect is that the ELI configuration allows one to trade area and speed, provided required number of receivers are available.

5 ADVANTAGES OF ELI

The basic reason we believe ELI gains an advantage is because the set of orthogonal voltage beams it creates allow it to use the same physical area and receivers to harvest photons from twice the solid angle that its linear dimensions would dictate.

ELI, like synthesis array, can only use coherent receivers. Therefore, one could have deployed the many, say 30, receivers as a synthesis instrument, fitting each to a modest, say 1 m, sized telescope and distributing them within an area of $\sim$100 m^2 to achieve similar resolution and FoV. The 1 m size limits the FoV to $\sim$10 arcmin at 100 GHz. The responsivity to distributed emission could be extended to $\sim$20 arcmin employing mosaicking and joint deconvolution methods. But, all these add to the complexity of data processing. On the other hand, ELI has natural responsivity to distributed emission. At higher frequencies, ELI is a better choice to map out diffuse emission than a synthesis telescope since, in the latter case, the primary beam shrinks further even with a modest collecting area.

As noted in the above section, a single dish requires some method of switching to ward off gain variations. When this is taken into account, ELI is faster. This applies to both continuum and spectral observations. Short-term gain variations being the limiting factor, single dishes are not the favourites for continuum observations. ELI betters single dishes in this perspective: since it cross multiplies the voltage signals from different receivers to form power spectra, to a large extent, it filters out receiver self-noise power.

Owing to the short-spacing sensitivity, the cross-power spectrum may include some atmospheric contributions. At low frequencies, this may be insignificant. At higher frequencies, atmospheric emission from the near field will be decorrelated. Some emission from higher atmosphere may still be left that may prove a problem for detecting smoothly distributed continuum emission (e.g. from dust or CMBR). One may have to go to high altitudes or space to avoid this limitation. For smoothly distributed spectral emission, the low-level continuum background may help calibrate the temperature scale.

The parabolic primary and relatively smaller area make ELI offer lesser air resistance and more economical to build, compared to a paraboloid. As an element in a synthesis array, it lends itself readily for close packing, allowing short-spacing measurements. On the other hand, ELI needs good off-axis optics performance, requires more complex back-end processor and may produce beams with higher side-lobe levels. We are building a prototype that will demonstrate both its benefits and challenges.

6 SUMMARY

We have presented a new cross telescope configuration, ELI, and have demonstrated that it is an effective way to use a large number of coherent receivers. It supports well observations of both point and extended sources, spectral and continuum. ELI allows us to trade survey speed and collecting area which gives it the ability to cover large FoV at modest sensitivity, useful in transient searches. It is economical to build, for a variety of reasons. As an interferometer element, ELI lends itself for close packing and blends short and long spacing visibilities naturally to provide low spatial frequency response, necessary for high-frequency arrays. We wish to first demonstrate its working in the 7–14 GHz range and then move up in frequency to explore the Galactic-plane molecular emission via simultaneous multiline transit surveys.

ACKNOWLEDGEMENTS

Author thanks the Raman Research Institute and the Department of Science and Technology, India for their unwavering support to this research and his colleagues at the Institute for encouragement and helpful comments. Author also thanks the anonymous referees whose comments have led to an improved manuscript.

REFERENCES

Balasubramanyam R., 2004, MNRAS, 354, 1189
Christiansen W. N., Hoegbom J. A., 1969, Radiotelescopes. Cambridge Univ. Press, Cambridge
Cohen R. J. et al., 2007, in Elmegreen B. G., Palous J., eds, Proc. IAU Symp. 237, Triggered Star Formation in a Turbulent ISM. Cambridge Univ. Press, Cambridge, p. 403
Condon J. J., Cotton W. D., Greisen E. W., Yin Q. F., Perley R. A., Taylor G. B., Broderick J. J., 1998, AJ, 115, 1693
Cornwell T. J., 1988, A&A, 202, 316
Dame T. M., Hartmann D., Thaddeus P., 2001, ApJ, 547, 792
Ekers R. D., Rots A. H., 1979, Astrophysics and Space Science Library, Vol. 76, Image Formation from Coherence Functions in Astronomy. Reidel, Dordrecht, p. 61
Goldsmith P. F., 1995, Emerson D. T., Payne J. M., eds, ASP Conf. Ser., Vol. 75, Multi-Feed Systems for Radio Telescopes. Astron. Soc. Pac., San Francisco, p. 337
Hacar A., Tafalla M., Kauffmann J., Kovács A., 2013, A&A, 554, A55
Hauser M. G. et al., 1998, ApJ, 508, 25

Heyer M. H., Brunt C., Snell R. L., Howe J. E., Schloerb F. P., Carpenter J. M., 1998, ApJS, 115, 241
Ivashina M., Bregman J. D., van Ardenne A., 2002, Proc. 12th Int. Conf. 'Microwave and Telecommunication Technology. A Way to Improve the Field of View of the Radiotelescope with a Dense Focal Plane Array. IEEE, p. 278
Jones P. A. et al., 2012, MNRAS, 419, 2961
Larson D. et al., 2011, ApJS, 192, 16
Melnick G. J., Tolls V., Snell R. L., Bergin E. A., Hollenbach D. J., Kaufman M. J., Li D., Neufeld D. A., 2011, ApJ, 727, 13
Meyer M. J. et al., 2004, MNRAS, 350, 1195
Payne J. M., 2002, Stanimirovic S., Altschuler D., Goldsmith P., Salter C., eds, ASP Conf. Ser. Vol. 278, Single-Dish Radio Astronomy: Techniques and Applications. Astron. Soc. Pac., San Francisco, p. 453
Payne J. M., Jewell P. R., 1995, Emerson D. T., Payne J. M., eds, ASP Conf. Ser. Vol. 75, Multi-Feed Systems for Radio Telescopes. Astron. Soc. Pac., San Francisco, p. 144
Planck Collaboration I, 2013, preprint (arXiv:1303.5062)
Sault R. J., Staveley-Smith L., Brouw W. N., 1996, A&AS, 120, 375
Schroeder D. J., 2000, Astronomical Optics. Academic Press, San Diego
Werner M. W. et al., 2004, ApJS, 154, 1

This paper has been typeset from a TEX/LATEX file prepared by the author.